Wave and Wind Effects on the Oxygen Transfer across an Air-Water Interface: An Experimental Study

Aldo Tamburrino* and Natalia Martínez

Department of Civil Engineering, University of Chile, Santiago, Chile

The results of an experimental study on the oxygen transfer across the air-water interface under the combined effect of wind and mechanically generated waves are presented in the paper. The experiments were carried out in a wind tunnel containing a water tank. From the analysis of the experimental data, a relationship for determining the gas transfer coefficient was obtained, and found that the mean square slope of the water waves, the wave celerity, the wind shear velocity, and the Schmidt number are the relevant variables involved in the phenomena. The results of this study can be considered as a contribution to the advancement of the phenomenon of reaeration in closed water bodies subjected to waves and wind, such as reservoirs and lakes.

Keywords: oxygen transfer, reaeration, water waves, wind generated waves, wind tunnel

INTRODUCTION AND OBJECTIVES

The quality of water bodies depends on the amount of dissolved oxygen (DO) that they contain. When there is a deficit of DO, a flux of oxygen across the free surface is generated, from the atmosphere to the water. Thus, it is of interest to know the oxygen transfer rate in order to predict the capacity of the water body to recover desirable DO concentrations. This process is named reaeration and often occurs under the presence of water waves generated by wind. Although it is known that both effects—wind and water waves—influence the gas transfer rate, a theory that fully describes and quantifies the reaeration in terms of wind shear stress, wave characteristics, near free surface turbulence, etc., does not exist yet. In this article, the results of an experimental study on the dependency of the reaeration coefficient with the combined effect of wind and mechanically generated water waves are presented. This superposition of effects seeks to emulate fetches longer than those that can be generated in laboratory wind-tunnels because the perturbation due to the wind on the main waves generates characteristics closer to those occurring in nature.

PREVIOUS RESEARCH

Gas transfer—particularly oxygen transfer—across the air-water interface of water bodies is an issue of the greatest importance because it is directly related to them. This phenomenon is also called reaeration and it is quantified by the oxygen transfer—or reaeration—coefficient, k_L. Several theories have been proposed to relate k_L with properties of the dissolved gas, the liquid, and the flow. The first one was the film theory, proposed by Nerst in 1904,[1] who postulated that there is a thin film at each side of the free surface where the mass transfer is molecular. The films have a constant thickness and are not transported by the flow. Outside of these films, the transfer is turbulent. Later, in 1935, Higbie[2] assumed that after the fluid at the free surface has reached a certain "age," it is replaced by fluid parcels coming from the bulk. Dankwerts[3] in 1951 proposed the surface renewal theory, in which the interface is composed by elements of fluids with different residence times which, in average, are renewed at a mean surface renewal rate r. In order to determine r, several conceptual theories have been developed. Fortescue and Pearson[4] proposed the large eddy model, in which the reaeration rate depends on the largest scales of turbulence. On the other hand, Lamont and Scott[5] proposed that the smallest eddies determine the gas transfer, and they linked the renewal rate to the viscous dissipation rate and the fluid viscosity. Both models relate r with a Reynolds number raised to an exponent, being the difference in the value of the exponent. The large dispersion of the measured data, especially field data, does not allow us to decide on one of the two models conclusively. Theofanus et al.[6] proposed a dual model, which considers that for flows with Reynolds numbers above a critical value the large eddy model is valid and for lower Reynolds numbers, Lamont and Scott's applies. Moog and Jirka[7] developed a model that included both scales in terms of the distribution of the turbulent dissipation rate near the interface. A detailed discussion on the value of the exponent of the Reynolds number can be found in their paper. In open channel flows, the reaeration coefficient has been related to the bursting phenomenon occurring on the bed.[8–11] Hanratty and colleagues[12–13] have shown that the most important kinematics variable in the gas transfer process is the vertical gradient of the vertical component of velocity, or surface velocity divergence (β). They linked the mass transfer coefficient to its frequency spectrum and to the spectrum of β, determining limit cases corresponding to low frequencies (larger structures), and high frequencies (smaller eddies). In any case, determination of the gas transfer coefficient requires measurements in order to close the relation between the reaeration coefficient and the turbulence characteristics. Gas transfer measurements in flumes demand channels sufficiently long to have gas concentration differences much greater than the

* *Author to whom correspondence may be addressed.*
E-mail address: atamburr@ing.uchile.cl
Can. J. Chem. Eng. 95:1594–1604, 2017

DOI 10.1002/cjce.22807
Published online 8 March 2017 in Wiley Online Library (wileyonlinelibrary.com).

uncertainties associated with the measurement process. In order to overcome this limitation, some researchers have utilized recirculating flumes[14–15,7] or moving bed flumes.[16] Long residence time can also be achieved in tanks containing water agitated by means of oscillating grids.[17–20] Agitation by means of one jet[21] or several small jets[22–23] has also been reported.

Regarding the gas transfer across the surfaces of such large water bodies as lakes, reservoirs, or the ocean when they are sheared by the wind, commonly k_L is related to the wind velocity measured at a certain height above the ground or water surface—usually at 10 m in field measurements (U_{10}),[24–28] 40 cm in laboratory setups,[29] or, more arbitrarily, the mean velocity in wind tunnels.[30] In order to avoid arbitrariness in the definition of the reference velocity, other researches use the friction velocity, u_*.[31–35] Studies on the effect that wind generated waves have on the mass transfer coefficient can be found, for example, in previous literature.[32,35–40] A summary and comparison among different formulas for estimating the reaeration coefficient due to wind in still water bodies are provided by Ro et al.[41] After the pioneering work of Downing and Truesdale[42] on the effect that mechanically generated waves have in the reaeration coefficient, several other authors have addressed the problem.[43–49] Jähne et al.[37–38] established the importance of gravity waves, which are characterized by their mean square slope, in the gas transfer process. Thais and Magnaudet[50] showed the validity of the use of a superposition of mechanically generated waves and wind waves as a way to achieve effective fetches longer than the water tank dimensions. It is observed that the reaeration coefficient grows dramatically with the wind velocity, such that $k_L \sim U_{10}^n$, with n around 0.5 for low velocities, and around 2 to 3 for high velocities.[51] This enhancement of the transfer coefficient is explained as some breaking occurs at higher wind velocities. According to Banerjee,[52] the good dependency between k_L and the friction velocity existing for lower velocities is not found for higher velocities because the microbreaking process begins to take place on the wave surface. When microbreaking exists, k_L is associated with the surface divergence, which is related to the mean square wave slope.[52] At some point, water waves can break, changing the leading mechanism of gas transfer. In this case, the transfer coefficient depends on the sea-state,[53] i.e. it depends on the wave statistics, including the wave height, period, and power spectrum. Other parameters like the windsea Reynolds number,[54–55] which is a Reynolds number in terms of the wind shear velocity and the angular frequency of the peak of the wave height spectrum, or a Reynolds number based upon the wind shear velocity and the wave characteristic height[55] are used to quantify k_L when breaking waves are present. It is interesting to note the unexpected weak dependence of k_L with U_{10} at high wind speeds reported in a study carried out in the North Atlantic,[56] a fact that could be related to the sea state. The experimental research reported in this paper is limited to non-breaking wave conditions.

The experimental setups used to determine the reaeration coefficient across the air-water interface considering a wind blowing tangential to the free surface consist basically in a combination of water channel and wind tunnel. Their dimensions are varied: For example, the setup used by McCready and Hanratty[57] was 9 m long and the water flow was 0.5 cm deep. The arrangement in the Institut de Mécanique Statistique de la Turbulence (Marsella, France) is 40 m long, the water depth is 1 m, and includes a wave maker.[58] Jähne et al.[38] carried out their studies in two circular tunnels whose perimeter, width, and maximum water depth were 1.57 m, 0.1 m, and 0.1 m and 11.6 m, 0.3 m, and 0.4 m, respectively. The advantage of the circular tunnels is that their fetch can be considered infinite.

EXPERIMENTAL SETUP AND METHODS

The experimental setup is sketched in Figure 1. It consists of four sections: the first comprises a centrifugal fan (Airolite, model VCL 085, with a 3 HP motor) with a rectangular output section of 1.0×0.8 m^2 (width $\times$ height), followed by a funnel in order to provide a smooth transition to the entrance of the wind tunnel, whose cross-section is 0.5×0.4 m^2. In order to smooth the flow and destroy large scale vortex structures, a honeycomb was installed at the beginning of the wind tunnel. To avoid vibrations transmitted from the fan to the wind tunnel, they are separated 7 cm and united by a flexible rubber band. The length of the wind-tunnel is 5.5 m and is followed by a water-tank 4 m long and 0.5 m deep. Finally, after the water tank there is a 0.5 m long final section with the same characteristics as the wind tunnel. The bottom of the wind tunnel is covered with sandpaper that defines a 0.2 mm roughness. Vertical walls and ceiling behave as aerodynamically smooth surfaces. Battens 5 mm high were installed at the beginning of the tunnel in order to accelerate the development of the boundary later, which was fully developed when it reached the water tank. The section comprising the water tank was made of transparent acrylic (1 cm width), facilitating visualization of the experiments and instrumentation arrangements. A wave generator was mounted in the upwind end of the water tank. It consisted of a paddle actioned by a motor. The wave frequency was controlled by the motor revolutions and the wave height by the stroke length of the paddle. In the opposite end of the tank, the reflection of the water waves was avoided by installing a beach consisting of an inclined, perforated plane.

Wind velocity profiles were measured with a 1-D hotwire (Extech, model 407123). This instrument measures in the range from 0.2 to 20 m/s, with a resolution of 0.1 m/s, a record rate of

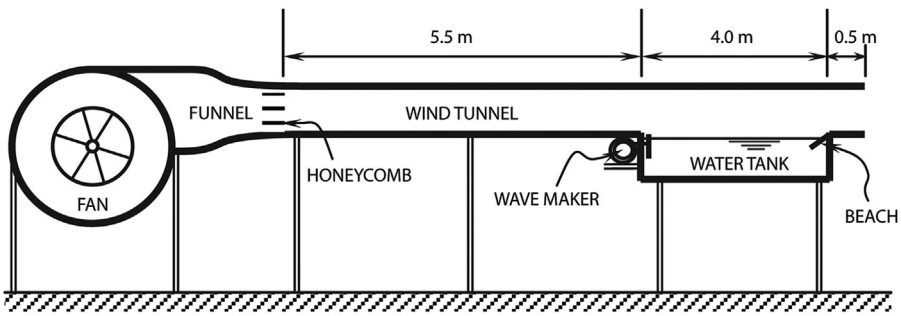

Figure 1. Sketch of the experimental setup.

0.5 Hz, and an accuracy of 3 % of the reading + 0.3 m/s, or 1 % of the full scale + 3 d, whichever is greater. The operating temperature range is 0 to 50 °C and environmental humidity can be up to 80 %. Data (velocity and temperature) were collected during 30 s, time that proved to be enough to get good mean velocity values. The data were stored in a computer for further analysis. The velocity profiles were measured at four locations along the water tunnel (0.8, 1.6, 2.4, and 3.2 m from the beginning of the water tank) and at 36 vertical positions. The velocity profiles near the water surface follow the logarithmic distribution, as has been shown elsewhere for this facility.[34,35] The velocity of the free surface was determined tracking the displacement of tracers (lettuce seeds) poured on the water surface. The tracers were recorded with a CCD camera FOR.A model VFC-300 with a macro zoom lens KOWA model LMZ503M. The data record rate was between 30 to 90 frames per second (depending on the wind velocity) at 512 × 512 pixels. The water surface elevation and its slope were measured at the same locations as the wind velocity profiles by means of two capacitive wave height gauges model WG-50 made by RBR operating in a master/slave format to avoid interference. The gauges were separated 6 mm from each other, a distance that ensures that there is no cross-talking between the sensors.[35,59] According to the maker, the accuracy is of 0.4 %, with a frequency response of 500 Hz. The slope was computed as the difference of water elevation recorded by the height gauges divided by the distance between them. The data were stored in a computer at a sampling rate of 100 Hz. The two time series of the water elevation and the slope were recorded, with a sampling time of 5 min per location. Jähne et al.[37,38] studied the dependency of the gas transfer across the air-water interface with the slope and found that the gas exchange rate is not simply controlled by the slope of capillary waves, but it depends on the total mean square slope when wind generated waves are present. Thus, slopes computed as $s \approx (\eta_1 - \eta_2)/\Delta x$ where η_1 and η_2 are the water surface elevations measured by each of the gauges separated a distance $\Delta x = 6$ mm can provide the necessary resolution to characterize the water wave properties involved in the gas transfer phenomenon.

Dissolved oxygen (DO) and temperature in the water body were recorded at a rate of 1 Hz with an oxygen meter by WTW, composed by a sensor model TriOximatic 300 and a microprocessor Oxi 3000. The resolution of the device for the DO measurements is 0.01 mg/L and its accuracy is 0.5 % of the measured value. The temperature measurements are provided with an accuracy of ±0.1 °C. Before each experiment, water was deoxygenated by adding sodium sulphite to the water tank. Depending on the experimental conditions, measurements lasted between 2 and 8 h. From the time series of the concentration, the gas transfer coefficient, k_L, was determined and standardized to 20 °C and 101 kPa according to the ASCE guidelines.[60]

The gas transfer coefficient (obtained from the concentration records), the free surface level, slope and velocity, and the wind shear velocity (computed from the logarithmic velocity distribution) were determined from the experiments under different conditions of wind velocity, frequencies, and wave heights of mechanically generated water waves. The experiments were determined by six conditions of wind velocities (no wind and five average nominal wind velocities in the tunnel), and five frequencies (no mechanical wave and four nominal frequencies). Due to the difficulty of setting a specific wave height, four ranges of wave heights were defined, in addition to the condition of no mechanically generated waves. In order to facilitate the presentation of the data, the velocities were labelled as V_{a_V}, where a_V: 0, ..., 5; the frequencies as F_{a_F}, with a_F: 0, 1, 1.5, 2, 3, and the wave heights as H_{a_H}, with a_H: 0, ..., 4. The values of the physical variables associated to the notation before mentioned are presented in Table 1.

RESULTS

A summary of the flow conditions and the characteristic parameters resulting of each test is presented in the Appendix. The table also includes the uncertainty associated to each variable.

Free Surface Velocity

From the analysis of the particle tracking of the tracers, the mean free surface u_S was obtained for the different experimental conditions and they are summarized in Table A1 in the Appendix.

Wind Shear Velocity

Examples of the velocity profiles along the water tank, for two sets of wind velocities and wave frequencies, are presented in Figure 2. The wind shear velocity, u_*, and the aerodynamic roughness, z_0, were obtained fitting the near free surface portion of the data to the logarithmic distribution given by Equation (1),

$$\frac{u - u_S}{u_*} = \frac{1}{\kappa}\ln\left(\frac{z}{z_0}\right) \tag{1}$$

where u is the wind velocity measured at a distance z from the free surface and $\kappa = 0.4$ is the constant of von Kármán. The values of u_* and z_0 for the different experimental conditions are presented in Table A1 in the Appendix. Because an overall value of the gas transfer coefficient will be calculated, the quantities given in the table correspond to the mean values (averaged over the free surface). The value of z_{max} used in Figure 2 to make dimensionless the vertical axis depends on the experiment is also presented in Table A1. The closest location to the water surface where the velocity was measured depended on the wave amplitude, ranging from 0.8 cm when no mechanical waves were generated up to 6.1 cm for 4.5 cm amplitude waves (i.e. the measurement was taken at 1.6 cm from the wave crest).

Characteristics of the Free Surface

The elevation of the free surface, η, was referred to its mean value. From the time series of η, its root mean square value, $\eta_{rms} = \sqrt{\overline{\eta^2}}$, was computed at each of the locations where the velocity distribution were measured (the overbar – denotes time average). The slope, $s = \partial\eta/\partial x$, was also recorded and its mean square value calculated, $s_{rms} = \sqrt{\overline{s^2}}$. In the same way as for wind shear velocity,

Table 1. Notation used to identify the experiments

Nominal wind velocity (m/s)		Frequency of mechanically generated waves (Hz)		Range of height of mechanically generated waves (cm)	
V0	No wind	F0	No waves	H0	No waves
V1	3.6	F1	1	H1	<1.5
V2	6.6	F1.5	1.5	H2	1.5–2
V3	7.9	F2	3	H3	2–2.5
V4	9.1	F3	3	H4	>2.5
V5	11.1				

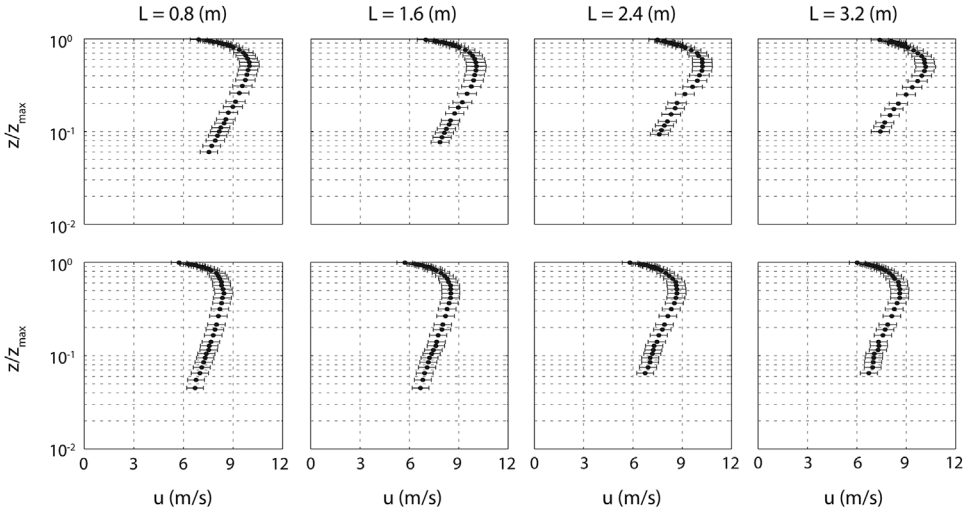

Figure 2. Examples of wind velocity profiles measured along the tank. The upper panels correspond to the experimental conditions labelled as V4F1H1 and the lower panels correspond to V3F2H1. Location along the tank is given by the value of L indicated above each column of figures.

the values of η_{rms} and s_{rms} used to correlate with the mass transfer coefficient correspond to the values averaged over the free surface. As an example of the time series of the water surface elevation and its slope, a portion of the record for one of the experiments is presented in Figure 3.

In order to compute a representative peak frequency of the water waves, the spectral analysis made by Longo[61] was applied to the elevation time series. The degree of freedom of the power spectra obtained is 30 and as an example, two of them are presented in Figure 4. Figure 4a corresponds to the case of only wind, for an experiment with an associated shear velocity $u_* = 0.43$ m/s (test V3F0H0, at 2.4 m from the beginning of the water tank). The spectrum obtained from one experiment with the combined effect of wind and mechanically generated waves (test V3F3H1) is presented in Figure 4b. In this case, $u_* = 0.34$ m/s and characteristic wave height (without wind) $\eta_{rms} = 4.2$ mm. The difference between boths cases is evident and reflects the origin of the energy that distorts the free surface, as shown by Rhee et al.[62] For the experimental conditions of Figure 4, it is observed that the mecanically generated waves overrun those generated by wind, without distinguishing the contribution of the wind in Figure 4b. This is not always the case, and there are occasions where the wind contribution to the waves is of the same order or higher than that due to the mechanical effect. An example is what happens for the test V3F1H1, whose spectrum of the free surface elevations recorded at the same location as those of Figure 4 are shown in Figure 5. In this case, the frequency associated to the peak of the spectrum of pure wind waves ($u_* = 0.34$ m/s) is around 5 Hz and the frequency of the mechanically generated waves is 1 Hz, with $\eta_{rms} = 3.7$ mm. A nonlinear interaction between them is observed, with the maximum energy not associated to the frequency $f_m = 1$ Hz (as in Figure 4b), but at near to 3 Hz. In this spectra, the segmented gray line indicates the frequency associated to the seiche that can be generated in the water tank, $f_S = \sqrt{gh}/(2L) = 0.27$ Hz, where g is the aceleration due to gravity, h is the water depth, and L is the length of the tank.

Overall quantities representative of the complete tank will be computed and used to correlate the (overall) gas transfer coefficient in the following sections of the paper. The values of f_P, η_{rms}, and s_{rms} presented before were computed in the four locations along the tank where the capacitive gauges were located (at 0.8, 1.6, 2.4, and 3.2 m from the beginning of the tank). Denoting with the subindex i the location of the gauges and calling A_i the area associated to the location i, the surface average of η_{rms} and the quadratic mean wave slope, s^2_{rms}, are defined respectively as follows:

$$\langle \eta_{rms} \rangle = \frac{\sum_{i=1}^{4} \eta_{rmsi} A_i}{\sum_{i=1}^{4} A_i} \tag{2}$$

$$\langle s^2_{rms} \rangle = \frac{\sum_{i=1}^{4} s^2_{rms} A_i}{\sum_{i=1}^{4} A_i} \tag{3}$$

For waves without wind, the dominant frequency of the waves is the same independent of the location along the tank and it corresponds to the frequency of the paddle, f_m. For waves due to the wind, the dominant frequency changes with the distance from the beginning of the tank. In most of the experiments, the frequency associated to the mechanically generated waves dominates over the wind waves along the tank, and the frequency associated to the peak is practically the same as f_m. However, in the experiments with stronger winds, the peak of the spectrum

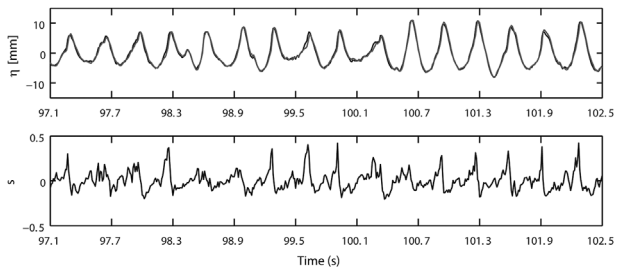

Figure 3. Portion of a record of the water surface level η (upper panel) and its slope s (lower panel). Experimental conditions correspond to the test labelled as V3F3H1. Two curves are presented in the upper panel, corresponding to each of the two water level sensors.

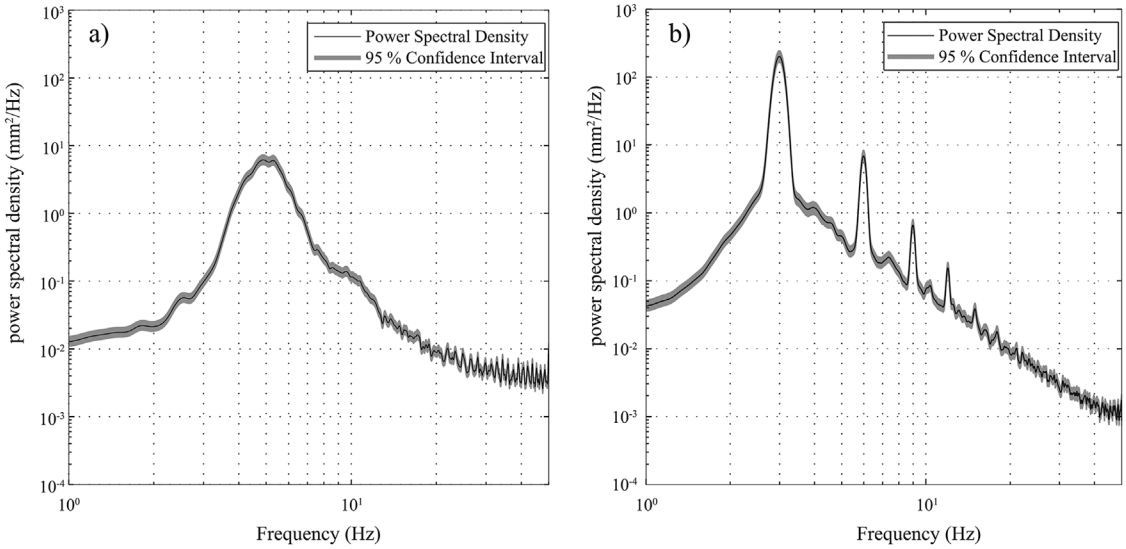

Figure 4. Spectra of water elevation at 2.4 m from the beginning of the water tank. (a) Only wind, $u^* = 0.43$ m/s. (b) Wind with $u^* = 0.34$ m/s superposed to mechanically generated waves with a frequency $f_m = 3$ Hz and characteristic height (without wind) of $\eta_{rms} = 4.2$ mm.

does not coincide with f_m (or one of its multiples). In order to take into account the variability of the peak frequency along the tank, an average peak frequency f_P is defined as follows:

$$\langle f_P \rangle = \frac{\sum_{i=1}^{4} f_{Pi} e_i A_i}{\sum_{i=1}^{4} e_i A_i} \tag{4}$$

where e_i is the spectrum energy density associated to the peak frequency f_{Pi}. In the following sections, these overall average values will be denoted without the angle brackets.

The characteristic wave height, H_S, was computed as the root mean square of the wave heights following the zero-crossing procedure used by Longo.[63]

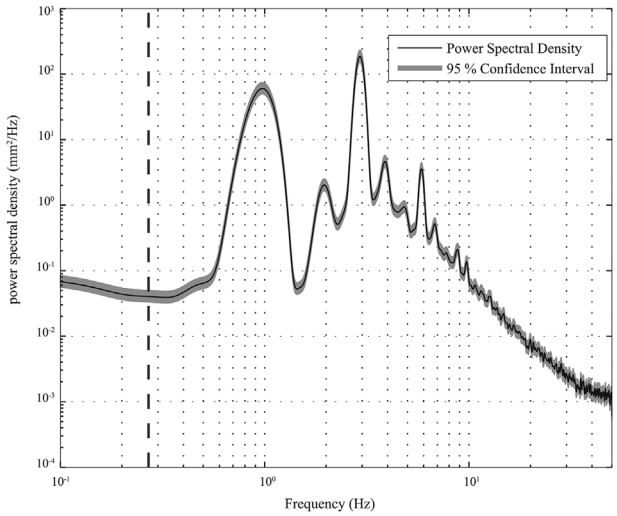

Figure 5. Spectra of water elevation of run V3F1H1 taken at 2.4 m from the begining of the water tank. Waves resulting fom the combined effect of wind ($u^* = 0.44$ m/s) and mechanically generated waves ($f_m = 1$ Hz, $\eta_{rms} = 3.7$ mm). The dashed gray line indicates the seiche frequency.

Determination of the Overall Oxygen Tranfer Coefficient

The oxygen transfer coefficient was computed from:[45,64,65]

$$\frac{\partial C}{\partial t} = k_L \frac{A}{V}(C_S - C) \tag{5}$$

In the equation above, C is the instantaneous concentration in the tank, C_S is the saturation concentration of oxygen in water, computed for the water temperature and ambient pressure according to the recommendations indicated by the European Inland Fisheries Advisory Commission (EIFAC).[66] A and V are the superficial area and water volume in the tank, respectively. The coefficient k_L was normalized at 20 °C by means of Arrhenius equation:[60,64,65]

$$k_{L20} = k_L \theta^{(20-T)} \tag{6}$$

where $\theta = 1.024$ and T is the temperature in °C. With C_0 as the initial oxygen concentration and h as the water depth in the tank,

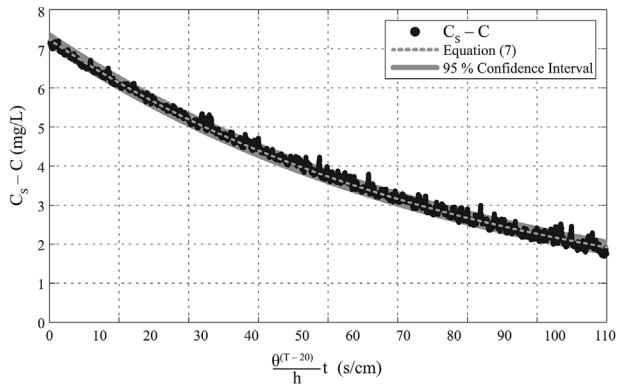

Figure 6. Evolution in time of the oxygen deficit concentration for run V2F2H1. Light dashed gray curve is the best fit of Equation (7) to the data. The error bar width is about the thickness of the data symbol and it cannot be distinguished in the graph.

integration of Equation (5) yields the following:

$$C_S - C = (C_S - C_0)\exp\left(-\frac{k_{L20}\theta^{(T-20)}}{h}t\right) \quad (7)$$

Using Matlab©, C_0 and k_{L20} were obtained from fitting the data to Equation (7) by means of a nonlinear least square algorithm. As an example, Figure 6 presents the experimental record and the best fitting curve (light dashed grey curve) for the experiment labelled as V2F2H1. A summary of the computed values of k_{L20} for the different flow conditions is given in the Appendix.

The diffusion coefficient of oxygen in water at the experiment temperature was computed using the expression of Wilke and Chang.[67] Computation of the dynamic viscosity and density of water at experiment temperature were computed from the relationships presented by White.[68]

DATA ANALYSIS

Comparison with Previous Data

In their study on the influence of waves on air-water gas transfer, Daniil and Gulliver[45] presented three relationships for the gas transfer coefficient:

$$k_L\sqrt{Sc} = 0.0159\,Hf, \quad k_L\sqrt{Sc} = 0.1148\,sHf,$$
$$k_L\sqrt{Sc} = 3.801\,s\sqrt{\nu f} \quad (8)$$

where H, f, and s are the characteristic height, frequency, and slope of the water waves, respectively. $Sc = \nu/D$ is the Schmidt number, with the kinematic viscosity of the water and D is the diffusion coefficient of the dissolved gas in water. Daniil and Gulliver performed experiments with mechanically generated waves, and their measurements are compared with those obtained in this research in Figure 7. The variables in the figure have dimensions of m/s in order to have the same kind of graphs as those presented in Daniil and Gulliver.[45] The straight lines correspond to the relation given by Equations (8). In the upper graph of Figure 7, the classical data obtained by Downing and Truesdale[42] and Hosoi et al.[43] are also shown.

For the case of gas transfer due to wind generated water waves, Jähne et al.[37] were pioneering in proposing that k_L depends on the total mean square slope of the water waves. The authors normalized the gas transfer coefficient to 20 °C and $Sc = 600$, $k_{L20-600} = k_{L20}\sqrt{Sc/600}$. The upper graph of Figure 8 shows the data obtained in this research for gas transfer due to wind generated waves, which were obtained in water tunnels by Jähne et al.,[37] together with the field data (also normalized to $Sc = 600$) presented by Frew et al.[39] in their study on air-sea gas transfer. As with Figure 7, this figure preserves the variables used by the authors in their original papers. In spite of the lack of dimensional homogeneity of the relationship, the correlation shown by the data is surprising, irrespective if they were obtained in the field or in different experimental facilities and experimental conditions. For completeness, in order to have the same graphs presented in Frew et al.,[39] the dependence of the gas transfer coefficient with the water shear velocity is also presented in Figure 8. Strictly speaking, the wind shear stress is transmitted to the water surface as skin friction and as drag due to the wave form and a proper value of u_{*water} should arise from measurements in the water. As no velocity measurements were taken from the water side in our

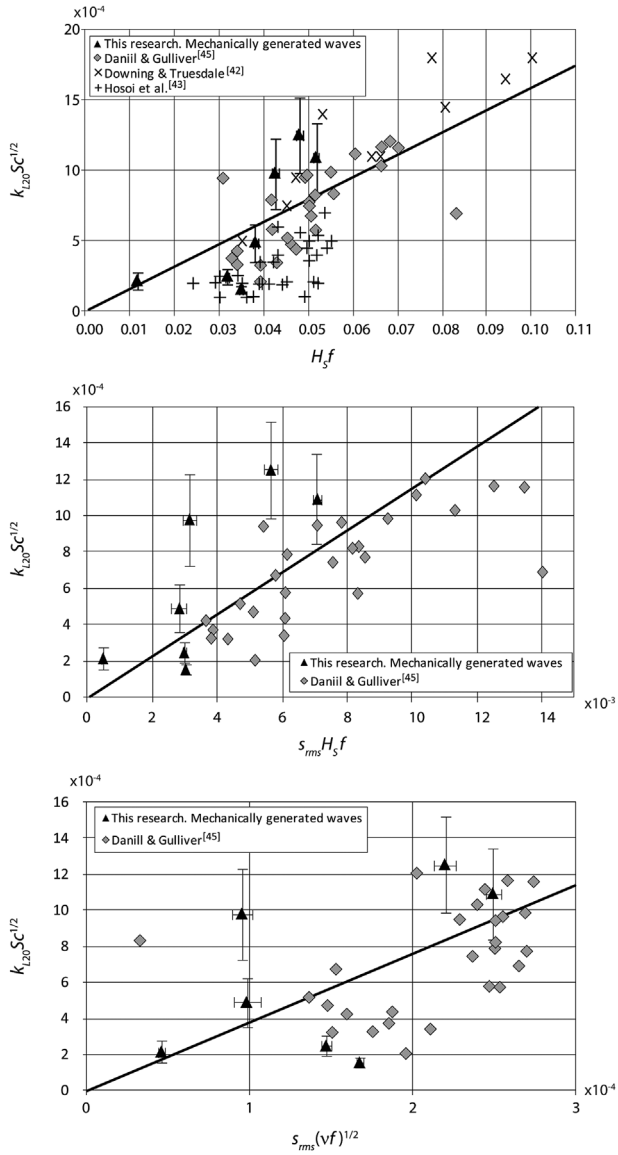

Figure 7. Gas transfer coefficient due to mechanically generated water waves. Comparison with the data presented in the study by Daniil and Gulliver[45] using the functional relationships presented in their paper, i.e. $k_{L20}\,Sc$ as function of $H_S\,f$ (upper graph), $s_{rms}H_S f$ (middle graph), and $s_{rms}\,(\nu f)$ (lower graph). Units of both axes are m/s. The straight line in each figure corresponds to the relationships given in Equation (8).

experiments, it was not possible to compute u_{*water} directly. However, following Frew et al.[39] and Jähne et al.[37] it was estimated as $u_{*water} = u_*\sqrt{\rho_{air}/\rho_{water}}$, where ρ stands for density. Hence, there is coherence in the lower graph of Figure 8, as all the authors computed the shear velocity in the same way.

Analysis of the Data Obtained in this Research

According to Danckwerts' renewal theory,[3] the gas transfer rate depends on the gas diffusion coefficient, D, and the renewal rate, r. Dimensional homogeneity indicates the following:

$$k_L \sim \sqrt{Dr} \quad (9)$$

The renewal rate characterizes the flow dynamics near the free surface. Thus, it should depend on the wave characteristics, the

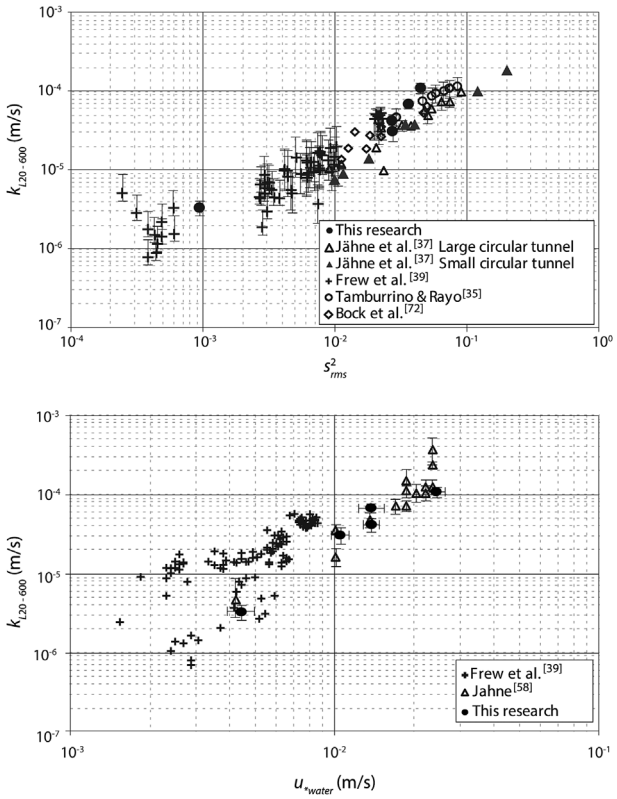

Figure 8. Gas transfer coefficient due to wind generated water waves. Comparison with data obtained in other studies. The upper graph shows the normalized gas transfer coefficient to 20 °C and Sc = 600 in terms of the mean square value of the slopes of the water waves. The lower graph shows the gas transfer coefficient in terms of the wind shear velocity referred to the water side. For some of the data obtained in this research, the uncertainty bar is covered by the symbol.

wind, and the fluid. Jähne et al.[38] showed the importance of the waves of large wavelengths in the gas transfer phenomenon (in contraposition to the limited contribution of capillary waves). Thus, f_P, η_{rms}, λ_P, and g are considered as the relevant variables that characterize r (λ_P is the wavelength associated to f_P). The wind is characterized by the friction velocity acting on the water surface, u_*, and the water is typified by its kinematic viscosity, ν. Thus, after applying the Buckingham's theorem, the following functional relationship is obtained:

$$\frac{r}{f_P} = \Phi\left(\frac{\lambda_P}{\eta_{rms}}, \frac{u_*}{\lambda_P f_P}, \frac{\lambda_P^2 f_P}{\nu}, \frac{\lambda_P f_P}{\sqrt{g\lambda_P}}\right) \tag{10}$$

It is proposed that the function Φ can be written as follows:

$$\Phi = \frac{\lambda_P^2 f_P}{\nu}\Phi_1\left(\frac{\lambda_P}{\eta_{rms}}, \frac{u_*}{\lambda_P f_P}, \frac{\lambda_P f_P}{\sqrt{g\lambda_P}}\right) \tag{11}$$

where the surface renewal is given by $r = \frac{\lambda_P^2 f_P^2}{\nu}\Phi_1$. The wave celerity associated to the peak is $c_P = \lambda_P f_P$. Furthermore, $\frac{\lambda_P}{\eta_{rms}}$ can be interpreted as a characteristic wave slope, and it can be represented by s_{rms}.

$$r = \frac{c_P^2}{\nu}\Phi_1\left(s_{rms}, \frac{u_*}{c_P}, \frac{c_P}{\sqrt{g\lambda_P}}\right) \tag{12}$$

Thus, Equation (9) becomes the following:

$$k_L \sim \sqrt{\frac{D}{\nu}c_P^2\Phi_1} \tag{13}$$

Recalling the Schmidt number, $Sc = \nu/D$, and calling $\Phi_2 = \sqrt{\Phi_1}$, the dimensionless gas transfer coefficient is given by the following:

$$\frac{k_L}{c_P}\sqrt{Sc} \sim \Phi_2, \tag{14}$$

where $\Phi_2 = \Phi_2\left(s_{rms}, \frac{u_*}{C_P}, \frac{C_P}{\sqrt{g\lambda_P}}\right)$. It is noted that $\sqrt{g\lambda_P}$ is proportional to the celerity of a deep water wave of wavelength λ_P, given by $c_{DWW} = \sqrt{\frac{g\lambda_P}{2\pi}}$. Thus, the ratio $\frac{C_P}{\sqrt{g\lambda_P}}$ corresponds to $\frac{C_P}{C_{DWW}} \sim \frac{1}{\sqrt{2\pi}}\tanh\left(2\pi\frac{h}{\lambda_P}\right)$. The experimental data gives $\frac{1}{\sqrt{2\pi}}\tanh\left(2\pi\frac{h}{\lambda_P}\right) = 0.399$, except for two experimental conditions where it takes the value 0.392. As the ratio $\frac{C_P}{\sqrt{g\lambda_P}}$ takes a constant value in the experiments, it can be dropped from the functional relationship Φ_2. Further, considering that $k_L\sqrt{Sc}$ is well correlated with s^2_{rms},[38] it is proposed that $\Phi_2\left(s_{rms}, \frac{u_*}{C_P}\right) = s^2_{rms}\Psi\left(\frac{u_*}{C_P}\right)$.

The function Ψ has to behave reasonably well for characteristic values of u_*/c_P, without cancelling or getting indeterminate. Without wind ($u_* = 0$), the gas transfer phenomenon is due only to the mechanically generated waves and $k_L\sqrt{Sc}$ should depend only on the water wave characteristics, then Ψ should take a constant value (arbitrarily set equal to 1). Similarly, if there are not mechanically generated waves and the wind is the only agent responsible of the surface renewal, wave frequency, and height are the exclusive result of u_*, and Ψ should take a finite value. With these considerations, the following function is Ψ proposed:

$$\Psi = \left[1 + a\left(\frac{u_*}{c_P}\right)^n\right]^m \tag{15}$$

where a, n, and m are parameters that should be obtained from the experimental data. Thus, the relation for the gas transfer coefficient is given by the following:

$$\frac{k_L}{c_P}\sqrt{Sc} = \alpha s^2_{rms}\left[1 + a\left(\frac{u_*}{c_P}\right)^n\right]^m \tag{16}$$

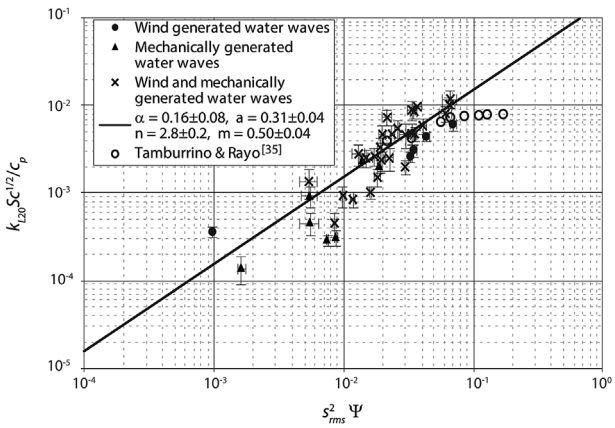

Figure 9. Dimensionless gas transfer coefficient. Experimental data and Equation (16).

The experimental data and the fit of Equation (16) to them are presented in Figure 9. The parameters involved in the equation take the values $\alpha = 0.16 \pm 0.08$, $a = 0.31 \pm 0.04$, $n = 2.8 \pm 0.2$, and $m = 0.50 \pm 0.04$.

CONCLUSION

As the oxygen transfer across the air-water interface is water-side controlled, it should depend on the flow characteristics of the water near the free surface. Studies on the flow structure in the water side when waves are present are rather limited, and many of them have been focused on strong turbulence.[69] Longo[63,70] analyzed the structure near the free surface when it was distorted by waves generated by a Crump weir and concluded that the most appropriate length and velocity scales for the description of the boundary layer in the water side, near the interface, are the root mean square of the free surface elevation (η_{rms}) and the root mean square of the vertical free surface velocity,[63] i.e. the scales can be computed from the free surface statistics. On the other hand, the most important kinematic variable that controls the gas transfer is the surface divergence, which is related to the root mean square of the free surface slope. Thus, the latter may serve as a proper substitute in the mass transfer analysis,[52] as has been shown by the good correlations between k_L and s_{rms} found in this research and others.[37–39,71]

In the experimental study reported in this article, water waves were generated by wind and mechanically with a wave maker. The superposition of both waves mimics the effect of fetches much longer than those that can be obtained in traditional laboratory setups when waves are the result of only wind,[50] thereby facilitating the experimental work.

Although the oxygen transfer across the wavy air-water interface addressed in this paper is far from being completely solved, and it is still necessary to continue investigating the subject, the results of this study are a contribution to the advancement of the phenomenon of reaeration in closed water bodies subjected to waves and wind, such as reservoirs and lakes.

The coupling of wind and mechanically generated waves is not a simple one, as can be observed in the spectra of water elevation, which show changes in the dominant frequency, depending on the wind intensity relative to the mechanically generated waves. Overall parameters quantifying the water waves were defined for the peak of the spectrum, and correlated with the gas transfer coefficient, in conjunction with the mean square value of the wave slopes. The wind effect was characterized by its shear velocity.

The experimental results obtained for only wind or only mechanical water waves were compared with others considered as classics in the literature, and using the same dimensional variables used by the original researchers. In the case only mechanical, the data follows the tendency reported in those studies, within the dispersion band that usually characterizes the gas transfer measurements. The only wind wave results show a perfect correlation (with small dispersion) between the transfer coefficient and the mean square slope of the water waves, with most of the present data falling over the previous one. When the gas transfer coefficient is correlated with the wind shear stress, the data present more dispersion, although they are contained within the previously reported data band.

The gas transfer due to the combined effect of wind and mechanically generated water waves was analyzed in conjunction with the only wind and only mechanical waves in order to obtain a general relationship that includes all the cases. With the aid of dimensional analysis and heuristic reasoning, a functional relationship between the gas transfer coefficient and the variables involved in the phenomena was obtained. According to this result, the mean square slope, the wave celerity, the wind shear velocity, and the Schmidt number are the relevant variables that characterize the gas transfer coefficient. The data show the usual dispersion found in gas transfer correlations.

ACKNOWLEDGEMENTS

The authors acknowledge the financial support provided by the Chilean Fund for Science and Technology, FONDECYT, by means of the grant N° 1020822.

NOMENCLATURE

A	superficial area of the tank (m^2)
A_i	area associated to the location i (m^2)
C	instantaneous bulk oxygen concentration
C_0	initial concentration of oxygen in the water tank
C_S	saturation concentration of oxygen in water
D	diffusion coefficient (m^2/s)
H	characteristic height (m)
H_S	characteristic wave height (m)
L	length of the tank (m)
$Sc = \nu/D$	Schmidt number
T	temperature (°C)
U_{10}	wind velocity measured at 10 m above the surface (m/s)
V	volume of water in the tank (m^3)
a	parameter of Equation (15)
c_P	wave celerity associated to f_P (m/s)
c_{DWW}	celerity of a deep water wave (m/s)
e	water elevation spectrum energy density associated to f_P (m^2/Hz)
f	characteristic frequency (Hz)
f_m	frequency of the mechanically generated water waves (Hz)
f_P	frequency associate to the peak of the spectra of water elevation (Hz)
f_s	frequency associated to the seiche (Hz)
g	acceleration due to gravity (m/s^2)
h	water depth (m)
k_L	gas transfer coefficient (m/s)
k_{L20}	gas transfer coefficient normalized at 20 °C (m/s)
$k_{L20-600}$	gas transfer coefficient normalized at 20 °C and $Sc = 600$ (m/s)
m	parameter of Equation (15)
n	parameter of Equation (15)
r	surface renewal rate (1/s)
s	free surface slope, characteristic slope in Equation (8)
s_{rms}	root mean square of the water surface slope
t	time (s)
x	distance along the axis of the tunnel (m)
u	wind velocity (m/s)
u_S	mean free surface velocity (m/s)
u_*	wind shear velocity (m/s)
u_{*water}	water-side free surface shear velocity (m/s)
z	vertical distance form the free surface (m)
z_0	aerodynamic roughness (m)
z_{max}	distance from the mean water surface to the top of the wind tunnel (m)
Φ	functional relationship

Φ_1	functional relationship
Φ_2	functional relationship
Ψ	functional relationship
Δx	separation of water surface elevation gauges (m)
α	parameter of Equation (16)
β	surface velocity divergence (1/s)
η	water surface elevation (m)
η_i	water surface elevation at location i (m)
η_{rms}	root mean square of the water surface elevation (m)
κ	von Kármán constant
λ_P	wavelength associated to f_P (m)
υ	kinematic viscosity (m^2/s)
ρ_{air}	air density (kg/m^3)
ρ_{water}	water density (kg/m^3)

APPENDIX

Table A1. Summary of experimental conditions and results U_X corresponds to the uncertainty of the variable X

V	F	H	k_{20} (cm/h)	$U_{k_{20}}$ (cm/h)	T (°C ± 0.1)	h (cm ± 0.1)	η_{rms} (mm)	$U_{\eta_{rms}}$ (mm)	S^2_{rms}	$U_{S^2_{rms}}$	f_P (Hz)	U_{f_P} (Hz)	H_{rms} (mm)	$U_{H_{rms}}$ (mm)
1	0	0	1.1	0.3	13.3	50.0	0.15	0.01	0.0009	0.0001	8.39	0.08	0.54	0.01
2	0	0	10.3	2.9	14.3	49.8	1.96	0.01	0.0271	0.0002	5.43	0.06	4.69	0.01
3	0	0	13.6	3.6	13.1	50.0	2.84	0.01	0.0268	0.0003	4.66	0.05	7.64	0.02
4	0	0	19.7	3.6	9.3	49.8	3.93	0.02	0.0358	0.0003	4.16	0.04	10.06	0.06
5	0	0	33.4	7.2	11.2	49.0	5.69	0.03	0.0443	0.0006	3.53	0.04	16.2	0.1
0	1	1	2.6	0.7	10.6	49.4	3.7	0.5	0.0016	0.0001	0.99	0.01	13	1
0	1.5	3	6.6	1.8	14.2	49.4	8.8	0.4	0.0055	0.0009	1.49	0.02	25	1
0	1.5	4	14.1	3.6	16.5	49.3	10.0	0.6	0.0054	0.0007	1.50	0.02	42	2
0	2	1	3.2	0.7	12.3	49.4	5.5	0.4	0.0087	0.0003	2.00	0.02	18	1
0	3	1	2.0	0.4	11.7	50.0	4.2	0.1	0.0074	0.0002	3.00	0.03	11.0	0.2
0	3	3	15.7	3.6	16.6	49.6	5.9	0.3	0.0187	0.0007	2.99	0.03	24	1
0	3	2	17.2	3.6	14.8	49.5	5.6	0.3	0.0139	0.0008	3.00	0.04	20.6	0.8
1	1	1	8.5	2.2	9.9	49.9	3.39	0.08	0.0084	0.0003	0.98	0.01	9.8	0.2
2	1	1	29.9	7.2	10.4	49.6	3.95	0.08	0.0145	0.0005	2.18	0.02	14.3	0.2
3	1	1	42.2	10.8	10.8	49.4	5.3	0.1	0.0186	0.0008	2.72	0.03	21.2	0.3
4	1	1	57.2	14.4	11.4	49.8	6.8	0.3	0.029	0.001	2.98	0.03	25.4	0.8
5	1	1	81.5	2.2	12.0	48.7	7.7	0.3	0.028	0.002	2.58	0.03	34.9	0.9
1	1.5	3	13.5	3.6	14.3	49.6	8.8	0.2	0.0097	0.0005	1.50	0.02	26.8	0.6
3	1.5	3	36.3	10.8	14.3	49.6	9.6	0.5	0.022	0.001	1.49	0.02	32	1
5	1.5	3	68.6	18.0	14.2	49.3	12.2	0.9	0.031	0.002	1.49	0.02	44	3
1	1.5	4	20.2	7.2	15.6	49.2	10.9	0.6	0.0053	0.0008	1.50	0.02	44	2
3	1.5	4	41.8	10.8	15.4	49.4	12.6	0.9	0.013	0.001	1.49	0.02	54	3
5	1.5	4	69.9	21.6	15.8	48.2	15	1	0.025	0.002	1.50	0.02	62	3
1	2	1	8.8	2.2	12.8	49.4	4.6	0.2	0.0116	0.0005	2.00	0.02	17.7	0.6
2	2	1	24.8	7.2	12.9	49.7	6.4	0.1	0.019	0.001	2.00	0.02	21.6	0.3
3	2	1	26.9	7.2	12.7	49.4	6.3	0.2	0.0168	0.0008	2.00	0.02	22.6	0.6
4	2	1	54.1	14.4	11.3	49.6	7.2	0.2	0.024	0.001	2.00	0.03	24.6	0.7
5	2	1	91.2	25.2	12.3	48.2	10.2	0.3	0.028	0.002	1.99	0.03	37.9	0.8
1	3	1	6.5	1.4	9.7	49.8	5.4	0.1	0.0158	0.0003	3.01	0.03	13.0	0.4
2	3	1	12.8	3.2	9.9	49.8	7.13	0.05	0.0288	0.0007	3.00	0.03	21.5	0.1
3	3	1	31.1	7.2	10.7	49.8	8.04	0.08	0.0334	0.0008	2.99	0.03	23.2	0.2
4	3	1	37.6	10.8	9.9	49.8	8.8	0.2	0.033	0.001	3.00	0.03	30.0	0.6
5	3	1	54.0	14.4	11.4	49.2	10	2	0.038	0.001	3.00	0.03	34	4
1	3	3	35.7	10.8	15.8	49.5	7.2	0.3	0.0228	0.0009	2.99	0.03	27.4	0.9
3	3	3	54.2	14.4	15.3	49.3	7.3	0.2	0.0181	0.0009	3.00	0.03	28.8	0.7
5	3	3	86.0	25.2	14.2	49.7	9.2	0.3	0.035	0.001	3.00	0.03	34.0	0.8
1	3	2	11.2	3.2	14.9	49.7	6.2	0.4	0.018	0.001	3.00	0.03	25	1
3	3	2	34.4	10.8	14.7	49.9	7.8	0.2	0.0176	0.0009	2.99	0.03	29.5	0.5
5	3	2	73.8	21.6	14.0	49.7	9.0	0.3	0.035	0.002	2.99	0.03	34.3	0.7

V	F	H	u_* (m/s)	U_{u_*} (m/s)	z_0 (mm)	U_{z_0} (mm)	u_s (m/s)	U_{u_s} (m/s)	z_{max} (cm ± 0.1)	D (m^2/s)	U_D (m^2/s)	ν (m^2/s)	U_ν (m^2/s)
1	0	0	0.14	0.02	0.0037	0.00	0.10	0.01	40.0	1.606×10^{-9}	4×10^{-12}	1.203×10^{-6}	3×10^{-9}
2	0	0	0.33	0.02	0.05	0.02	0.14	0.01	40.0	1.652×10^{-9}	4×10^{-12}	1.174×10^{-6}	3×10^{-9}
3	0	0	0.43	0.03	0.04	0.02	0.19	0.01	40.0	1.597×10^{-9}	4×10^{-12}	1.210×10^{-6}	3×10^{-9}
4	0	0	0.43	0.05	0.07	0.07	0.28	0.01	40.0	1.418×10^{-9}	4×10^{-12}	1.343×10^{-6}	4×10^{-9}
5	0	0	0.76	0.05	0.37	0.11	0.36	0.01	40.0	1.504×10^{-9}	4×10^{-12}	1.275×10^{-6}	4×10^{-9}
0	1	1	–	–	–	–	0.00	0.01	–	1.475×10^{-9}	4×10^{-12}	1.297×10^{-6}	4×10^{-9}
0	1.5	3	–	–	–	–	0.01	0.01	–	1.650×10^{-9}	4×10^{-12}	1.175×10^{-6}	3×10^{-9}

(*Continued.*)

Table A1. (*Continued*)

V	F	H	u_* (m/s)	U_{u_*} (m/s)	z_0 (mm)	U_{z_0} (mm)	u_s (m/s)	U_{u_s} (m/s)	z_{max} (cm ± 0.1)	D (m^2/s)	U_D (m^2/s)	ν (m^2/s)	U_ν (m^2/s)
0	1.5	4	–	–	–	–	0.01	0.01	–	1.765×10^{-9}	5×10^{-12}	1.108×10^{-6}	3×10^{-9}
0	2	1	–	–	–	–	0.01	0.01	–	1.555×10^{-9}	4×10^{-12}	1.238×10^{-6}	3×10^{-9}
0	3	1	–	–	–	–	0.02	0.01	–	1.527×10^{-9}	4×10^{-12}	1.258×10^{-6}	3×10^{-9}
0	3	3	–	–	–	–	0.05	0.01	–	1.771×10^{-9}	5×10^{-12}	1.104×10^{-6}	3×10^{-9}
0	3	2	–	–	–	–	0.01	0.01	–	1.678×10^{-9}	4×10^{-12}	1.158×10^{-6}	3×10^{-9}
1	1	1	0.16	0.02	0.01	0.01	0.08	0.01	40.1	1.445×10^{-9}	4×10^{-12}	1.321×10^{-6}	4×10^{-9}
2	1	1	0.39	0.03	0.08	0.05	0.16	0.01	40.7	1.469×10^{-9}	4×10^{-12}	1.302×10^{-6}	4×10^{-9}
3	1	1	0.44	0.03	0.13	0.05	0.18	0.01	40.9	1.488×10^{-9}	4×10^{-12}	1.287×10^{-6}	4×10^{-9}
4	1	1	0.59	0.05	0.30	0.14	0.21	0.01	40.4	1.513×10^{-9}	4×10^{-12}	1.268×10^{-6}	3×10^{-9}
5	1	1	0.86	0.08	0.77	0.43	0.32	0.01	41.5	1.541×10^{-9}	4×10^{-12}	1.248×10^{-6}	3×10^{-9}
1	1.5	3	0.22	0.03	0.07	0.06	0.06	0.01	40.6	1.651×10^{-9}	4×10^{-12}	1.174×10^{-6}	3×10^{-9}
3	1.5	3	0.46	0.04	0.15	0.10	0.17	0.01	40.7	1.652×10^{-9}	4×10^{-12}	1.174×10^{-6}	3×10^{-9}
5	1.5	3	0.79	0.07	0.60	0.26	0.37	0.01	40.9	1.650×10^{-9}	4×10^{-12}	1.175×10^{-6}	3×10^{-9}
1	1.5	4	0.22	0.03	0.10	0.08	0.07	0.01	41.4	1.721×10^{-9}	5×10^{-12}	1.132×10^{-6}	3×10^{-9}
3	1.5	4	0.51	0.06	0.24	0.18	0.15	0.01	40.9	1.708×10^{-9}	4×10^{-12}	1.140×10^{-6}	3×10^{-9}
5	1.5	4	1.1	0.1	1.81	0.91	0.27	0.01	41.0	1.729×10^{-9}	5×10^{-12}	1.128×10^{-6}	3×10^{-9}
1	2	1	0.18	0.02	0.04	0.04	0.07	0.01	40.6	1.578×10^{-9}	4×10^{-12}	1.222×10^{-6}	3×10^{-9}
2	2	1	0.28	0.03	0.01	0.01	0.12	0.01	40.3	1.583×10^{-9}	4×10^{-12}	1.219×10^{-6}	3×10^{-9}
3	2	1	0.37	0.03	0.02	0.01	0.19	0.01	40.6	1.574×10^{-9}	4×10^{-12}	1.225×10^{-6}	3×10^{-9}
4	2	1	0.54	0.06	0.13	0.11	0.21	0.01	40.5	1.507×10^{-9}	4×10^{-12}	1.273×10^{-6}	4×10^{-9}
5	2	1	0.84	0.06	0.80	0.29	0.34	0.01	42.1	1.556×10^{-9}	4×10^{-12}	1.237×10^{-6}	3×10^{-9}
1	3	1	0.14	0.01	0.01	0.00	0.06	0.01	40.0	1.436×10^{-9}	4×10^{-12}	1.329×10^{-6}	4×10^{-9}
2	3	1	0.25	0.02	0.01	0.00	0.13	0.01	40.0	1.444×10^{-9}	4×10^{-12}	1.322×10^{-6}	4×10^{-9}
3	3	1	0.34	0.03	0.03	0.02	0.17	0.01	40.0	1.482×10^{-9}	4×10^{-12}	1.292×10^{-6}	4×10^{-9}
4	3	1	0.62	0.06	0.39	0.20	0.27	0.01	40.0	1.444×10^{-9}	4×10^{-12}	1.322×10^{-6}	4×10^{-9}
5	3	1	0.9	0.1	1.12	0.87	0.26	0.01	40.0	1.514×10^{-9}	4×10^{-12}	1.267×10^{-6}	3×10^{-9}
1	3	3	0.27	0.06	0.33	0.48	0.08	0.01	40.7	1.728×10^{-9}	5×10^{-12}	1.129×10^{-6}	3×10^{-9}
3	3	3	0.57	0.09	0.40	0.40	0.20	0.01	40.7	1.702×10^{-9}	4×10^{-12}	1.143×10^{-6}	3×10^{-9}
5	3	3	1.1	0.1	1.38	0.94	0.23	0.01	40.5	1.650×10^{-9}	4×10^{-12}	1.176×10^{-6}	3×10^{-9}
1	3	2	0.22	0.02	0.09	0.05	0.07	0.01	40.4	1.682×10^{-9}	4×10^{-12}	1.155×10^{-6}	3×10^{-9}
3	3	2	0.49	0.03	0.28	0.13	0.24	0.01	40.2	1.674×10^{-9}	4×10^{-12}	1.160×10^{-6}	3×10^{-9}
5	3	2	1.1	0.1	1.70	0.77	0.27	0.01	40.6	1.639×10^{-9}	4×10^{-12}	1.182×10^{-6}	3×10^{-9}

REFERENCES

[1] E. L. Cussler, *Diffusion. Mass transfer in fluid systems*, 3rd edition, Cambridge University Press, New York **1991**, p. 282.

[2] R. Higbie, *T. Am. Inst. Chem. Eng*. **1935**, *31*, 365.

[3] P. V. Danckwerts, *Ind. Eng. Chem*. **1951**, *46*, 1460.

[4] G. E. Fortescue, J. R. A. Pearson, *Chem. Eng. Sci*. **1967**, *22*, 163.

[5] J. C. Lamont, D. S. Scott, *AIChE J*. **1970**, *16*, 513.

[6] T. G. Theofanous, R. N. Houze, L. K. Brumfield, *Int. J. Heat Mass Tran*. **1976**, *19*, 613.

[7] D. B. Moog, G. H. Jirka, *J. Hydraul. Eng.-ASCE* **1999**, *125*, 3.

[8] J. C. R. Hunt, *Gas transfer at water surfaces*, Springer-Science +Business Media, Berlin **1984**.

[9] S. Komori, Y. Murakami, H. Ueda, *J. Fluid Mech*. **1989**, *203*, 102.

[10] M. Rashidi, S. Banerjee, *Phys. Fluids* **1988**, *31*, 2491.

[11] M. Rashidi, *Phys. Fluids* **1997**, *9*, 3485.

[12] K. K. Sikar, T. J. Hanratty, *J. Fluid Mech*. **1970**, *44*, 589.

[13] M. A. McCready, E. Vassihadou, T. J. Hanratty, *AIChE J*. **1986**, *32*, 1108.

[14] E. L. Thackston, P. A. Krenkel, *J. Sanit. Eng. Div.- ASCE* **1969**, *95*, 65.

[15] Y. L. Lau, *Prog. Water Technol*. **1975**, *7*, 519.

[16] J. S. Gulliver, M. J. Halverson, *Water Resour. Res*. **1989**, *25*, 1783.

[17] W. Asher, J. Pankow, *Tellus* **1986**, *38B*, 305.

[18] C. R. Chu, G. H. Jirka, *Int. J. Heat Mass Tran*. **1992**, *35*, 1957.

[19] S. P. McKenna, W. R. McGillis, E. J. Bock, "Free-surface turbulence and air-water gas transfer," *1st International Symposium Turbulent and shear Flow Phenomena*, Santa Barbara, 12–15 September **1999**.

[20] N. Herlina, G. H. Jirka, *J. Fluid Mech*. **2008**, *594*, 183.

[21] A. A. Sonin, M. A. Shimko, J. H. Chun, *Int. J. Heat Mass Tran*. **1986**, *29*, 1319.

[22] M. Grisenti, J. George, "Hydrodynamics and mass transfer in a jet-agitated vessel," *Second International Symposium on Gas Transfer at Water Surfaces*, Minneapolis, 11–14 September **1990**.

[23] A. Tamburrino, C. Aravena, J. S. Gulliver, *Transport at the Air-Sea Interface*, Springer, Heildelberg **2007**, Chapter 5.

[24] R. Banks, *J. Env. Eng. Div.-ASCE* **1975**, *101*, 813.

[25] G. E. Mattingly, *J. Hyd. Eng. Div.-ASCE* **1977**, *103*, 311.

[26] R. Wanninkhof, *J. Geophys. Res*. **1992**, *C5*, 7373.

[27] J. Crusius, R. Wanninkhof, *Limnol. Oceanogr*. **2003**, *48*, 1010.

[28] R. Wanninkhof, W. E. Asher, D. T. Ho, W. R. McGillis, *Annu. Rev. Mar. Sci*. **2009**, 1213.

[29] T. V. Belanger, J. A. Meyer, M. G. von Canal, M. V. Desik, *Lake Reserv. Manage*. **1999**, *15*, 185.

[30] C. Zappa, W. Asher, A. Jessup, *J. Geophys. Res*. **2001**, *106*, 9385.

[31] S. Komori, R. Nagaosa, Y. Murakami, *J. Fluid Mech*. **1993**, *249*, 161.

[32] W. L. Peirson, J. W. Walker, C. H. Welch, M. L. Banner, "Defining the enhancement of air-water interfacial oxygen exchange rate due to wind-forced microscale waves," in *Transport at the Air Sea Interface*, C. S. Garbe, R. A. Handler, B. Jähne, Eds., Springer, Heildelberg **2007**, 117.

[33] C. R. Chu, G. H. Jirka, "Reaeration in combined wind/stream driven flows," in *Air-Water Gas Transfer*, B. Jähne, E. C. Monahan, Eds., AEON Verlag and Studio, Hanau **1995**, 79.

[34] A. Tamburrino, S. Rayo, Y. Niño, "Wind and water-turbulence effects on the reaeration coefficient in a water body," *Fifth International Symposium on Environmental Hydraulics*, ISEH V, Tempe, 4–7 December **2007**.

[35] A. Tamburrino, L. Rayo, "Effect of the slope of short fetch wind-driven waves on the oxygen transfer in a water body," *Sixth International Symposium on Environmental Hydraulics*, ISEH VI, Athens, 23–25 June **2010**.

[36] A. F. Eloubaidi, E. J. Plate, *J. Hyd. Eng. Div.-ASCE* **1972**, *98*, 153.

[37] B. Jähne, W. Huber, A. Dutzi, T. Wais, J. Imberger, "Wind/wave-tunnel experiment on the Schmidt number - and wave field dependence of air/water gas exchange," in *Gas Transfer at Water Surfaces*, W. Brutsaert, G. H. Jirka, Eds., Springer-Science+Business Media, B.V., Dordrecht **1984**.

[38] B. Jähne, K. O. Munich, R. Bosinger, A. Dutzi, W. Huber, P. Libner, *J. Geophys. Res*. **1987**, *92*, 1937.

[39] N. Frew, E. Bock, E. Schimpf, T. Hara, H. Hauβecker, J. Edson, W. McGillis, R. Nelson, S. McKenna, M. Uzb, B. Jähne, *J. Geophys. Res*. **2004**, *109*, 1.

[40] K. S. Ro, P. G. Hunt, *T. ASABE* **2006**, *49*, 1615.

[41] K. S. Ro, P. G. Hunt, M. E. Poach, *Crit. Rev. Env. Sci. Tec*. **2007**, *37*, 539.

[42] A. L. Downing, G. A. Truesdale, *J. Appl. Chem*. **1955**, *5*, 570.

[43] M. Hosoi, A. Ishida, K. Imoto, *Coast. Eng. J*. **1977**, *20*, 121.

[44] L. Merlivat, L. Memery, *J. Geophys. Res*. **1983**, *88*, 707.

[45] E. Daniil, J. S. Gulliver, *J. Environ. Eng.-ASCE* **1991**, *117*, 522.

[46] Z. Yin, Z. David, B. Liang, L. Wang, *J. Hydrodyn*. **2013**, *25*, 718.

[47] Z. Yin, N. Yu, B. Liang, J. Zeng, S. Xie, *Journal of Ocean University of China* **2016**, *15*, 78.

[48] M. T. Nguyen, S. K. Tan, *AIChE J*. **2013**, *59*, 4839.

[49] M. T. Nguyen, A. Appan, D. S. Tan, S. K. Tan, *J. Env. Eng.-ASCE* **2014**, 140.

[50] L. Thais, J. Magnaudet, *J. Fluid Mech*. **1996**, *328*, 313.

[51] D. Zhao, Y. Toba, Y. Suzuki, S. Komori, *Tellus B* **2003**, *55*, 478.

[52] S. Banerjee, "The Air-Water Interface: Turbulence and Scalar Exchange," *Transport at the Air-Sea Interface*, C. S. Garbe, R. A. Handler, B. Jähne, Eds., Springer, Berlin **2007**.

[53] D. K. Woolf, *Tellus B* **2005**, *57*, 87.

[54] Y. Toba, S. Komori, Y. Suzuki, D. Zhao, "Similarity and dissimilarity in air–sea momentum and CO2 transfers: the nondimensional transfer coefficients in light of the windsea Reynolds number," *WIT Transactions on State of the Art in Science and Engineering, 23*, WIT Press, Southampton **2006**.

[55] D. Zhao, L. Xie, *J. Oceanogr*. **2010**, *66*, 663.

[56] T. G. Bell, W. de Bruyn, S. D. Miller, B. Ward, K. Christensen, E. S. Saltzman, *Atmos. Chem. Phys*. **2013**, *13*, 11073.

[57] M. J. McCready, T. J. Hanratty, *AIChE J*. **1984**, *30*, 816.

[58] B. Jähne, T. Wais, L. Memery, G. Gaulliez, L. Merlivat, K. O. Münnich, M. Coantic, *J. Geophys. Res*. **1985**, *90*, 11989.

[59] L. Rayo, *Efecto de las ondas superficiales generadas por viento en la transferencia de oxígeno de un cuerpo de agua*, Civil Engineering Thesis, University of Chile, Santiago **2010**, p. 48.

[60] ASCE, *Measurement of Oxygen Transfer in Clean Water*, 2nd edition, ANSI-ASCE 2-91, ASCE, Reston **1992**.

[61] S. Longo, *Coast. Eng*. **2012**, *61*, 27.

[62] T. S. Rhee, P. D. Nightingale, D. K. Woolf, G. Caulliez, P. Bowyer, M. O. Andreae, *J. Geophys. Res*. **2007**, *112*, C05027.

[63] S. Longo, *Exp. Fluids* **2010**, *49*, 1325.

[64] R. B. Banks, L. Raschid-Sally, C. Polprasert, *J. Environ. Eng.-ASCE* **1983**, *109*, 232.

[65] A. R. Rao, *J. Environ. Eng.-ASCE* **1999**, *125*, 215.

[66] EIFAC (European Inland Fisheries Advisory Commission), *Flow-through and Recirculation Systems: Report of the working group on terminology, format and units of measurement as related to flow-through and recirculation system*, Technical Paper EIFAC/T49, ISBN: 9251024162, Food and Agriculture Organization of the United Nations, Rome **1986**.

[67] C. R. Wilke, P. Chang, *AIChE J*. **1955**, *1*, 264.

[68] F. M. White, *Fluid mechanics*, 4th edition, McGraw-Hill, New York **1998**.

[69] M. Brocchini, H. Peregrine, *J. Fluid Mech*. **2001**, *449*, 255.

[70] S. Longo, *Exp. Fluids* **2011**, *50*, 201.

[71] E. J. Bock, T. Hara, N. M. Frew, W. R. McGillis, *J. Geophys. Res*. **1999**, *104*(C11), 25821.

Manuscript received August 15, 2016; revised manuscript received December 14, 2016; accepted for publication December 20, 2016.